Inorganic Chemistry

Article

pubs.acs.org/IC

Ferrocene–Dithiolene Hybrids: Control of Strong Donor–Acceptor Electronic Communication to Reverse the Charge Transfer Direction

Tetsuro Kusamoto, Kenji Takada, Ryota Sakamoto, Shoko Kume, and Hiroshi Nishihara*

Department of Chemistry, School of Science, The University of Tokyo, 7-3-1 Hongo, Bunkyo-ku, Tokyo 113-0033, Japan

Supporting Information

ABSTRACT: We prepared a novel class of ferrocene–dithiolene hybrid molecules, $FcS_4dt(Me)_2$ and $FcS_4dt[Pt(^tBu_2bpy)]$ (where FcS_4dt indicates 2-(1,3-dithia[3]-ferrocenophane-2-ylidene)-1,3-dithiole-4,5-dithiolate and $^tBu_2bpy$ indicates 4,4′-di-*tert*-butyl-2,2′-bipyridine), in which the ferrocene moiety was bound to the planar conjugated dithiolene skeleton via two sulfur atoms such that the cyclopentadienyl rings were perpendicular to the dithiolene backbone. The physical properties and electronic structures of the complexes and their oxidized species $[FcS_4dt(Me)_2]^{\bullet+}$ and $[FcS_4dt[Pt(^tBu_2bpy)]]^{\bullet+}$ were investigated by means of single-crystal X-ray diffraction (XRD) analysis, cyclic voltammetry, electron paramagnetic resonance (EPR), and UV–vis near infrared (UV–vis–NIR) spectroscopy. The electron density distributions of the highest occupied molecular orbitals (HOMOs) of $FcS_4dt(Me)_2$ and $FcS_4dt[Pt(^tBu_2bpy)]$ differed remarkably in that the HOMO of the former was ferrocene-based whereas that of the latter was dithiolene-based. The differences in the HOMO distributions originated from the energy level of the dithiolene-based π-orbital in each of the complexes, which was controlled by changing R in $FcS_4dt(R)_2$ (R = Me for $FcS_4dt(Me)_2$; 2R = $Pt(^tBu_2bpy)$ for $FcS_4dt[Pt(^tBu_2bpy)]$). We succeeded in analyzing the crystal structure of $[FcS_4dt[Pt(^tBu_2bpy)]]$-$(F_4TCNQ)\cdot C_6H_{14}\cdot CH_2Cl_2$ (where F_4TCNQ indicates 2,3,5,6-tetrafluoro-7,7,8,8-tetracyanoquinodimethane), which provided a rare example of the crystal structure of a $[Pt(diimine)(dithiolate)]^{\bullet+}$ ion-based complex. A comparison of the bond lengths in $FcS_4dt[Pt(^tBu_2bpy)]$ and $[FcS_4dt[Pt(^tBu_2bpy)]]^{\bullet+}$ suggested that the latter complex displayed a conjugated dithiolene-based π-radical character. These considerations agreed well with the electronic structures calculated using density functional theory (DFT) and time-dependent(TD)-DFT methods. Significant electronic communication between the ferrocene and dithiolene moieties was detected for both $[FcS_4dt(Me)_2]^{\bullet+}$ and $[FcS_4dt[Pt(^tBu_2bpy)]]^{\bullet+}$ in the appearance of an intramolecular charge transfer band, which was hardly observed for previously reported ferrocene–dithiolene hybrid molecules. The charge transfer direction was reversed between the two cations. The electron coupling parameter H_{AB} and the potential energy curves of the oxidized complexes were estimated based on the classical two-state Marcus–Hush theory. These results suggest that FcS_4dt-based metalladithiolenes can exhibit controllable electronic structures expressed as double-minimum potential energy curves.

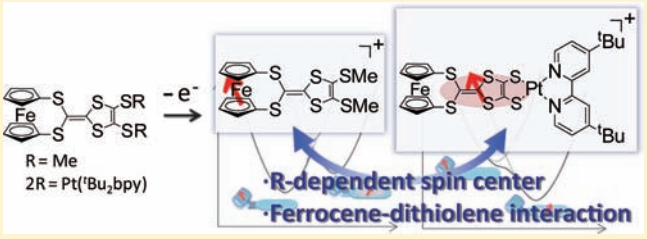

Molecules that exhibit redox properties have been studied extensively in recent decades as promising candidates for nanoscale devices and switches. One goal has been to achieve fine control over the physical properties of these materials by adding or removing electrons. Metalladithiolenes are an attractive molecular system for this purpose because they display multistep redox behavior, which, in some cases, accompanies the formation of a π-radical in which the spin density is delocalized over the π-conjugated molecular skeleton. Metalladithiolenes exhibit vivid physical properties,[1] such as magnetism, (super)conductivity, nonlinear optical properties, strong near-infrared (NIR) absorption, and fluorescence. The chemical properties[2] are interesting as well, including the reversible binding and release of olefins, cocatalytic activity toward water reduction, and radical quenching. Methalladithiolenes have therefore been examined as possible novel multifunctional molecular systems.

The physical and chemical properties of metalladithiolenes are based on their electronic structures; therefore, an understanding of the electronic structures is crucial for precisely controlling the properties of these compounds. Eisenberg and co-workers developed a series of Pt(diimine)(dithiolate) complexes, including $Pt(^tBu_2bpy)(tdt)$ ($^tBu_2bpy$ = 4,4′-di-*tert*-butyl-2,2′-bipyridine, tdt = toluene-3,4-dithiolate), shown in Chart 1. They achieved control over the emission and nonlinear optical properties through chemical modification of the ligands.[1h−j] Wieghardt et al. elucidated the electronic structures of bis-dithiolate complexes $M(bdt)_2^{n-}$ (n = 0, 1, 2; M = CrO, Fe, Co, Ni, Cu, Au, etc.) and related complexes, revealing that the character of the frontier orbitals depended strongly on the identity of the central metal.[3] We have established peculiar electronic structures of metalladithiolenes based on a TEMPO-bound dithiolene ligand, $tempodt(R)_2$ (TEMPO = 2,2,6,6-tetramethylpiperidine-l-oxy radical, R = CH_2CH_2CN).[1n,2d] $Tempodt(R)_2$ is composed of two electron-donating units;

Received: March 20, 2012
Published: May 30, 2012

   dx.doi.org/10.1021/ic300581a | *Inorg. Chem.* 2012, 51, 12102–12113

Chart 1

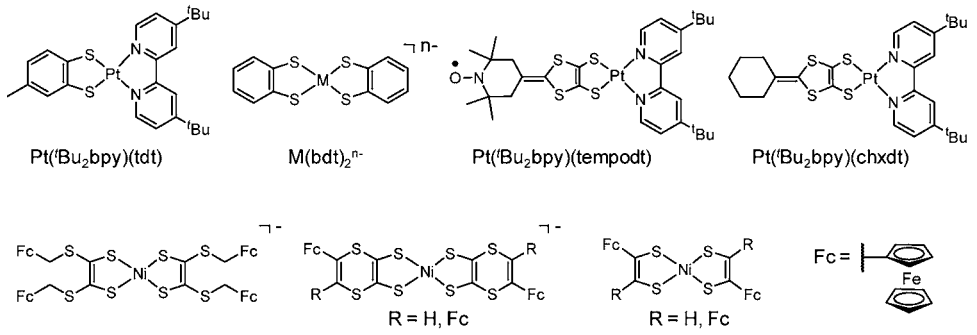

TEMPO, a stable organic radical having a spin of $S = 1/2$ and a dithiafulvene unit (π-conjugated dithiolene unit), which is half structure of a TTF (= tetrathiafulvalene) molecule. The coordination of tempodt to Pt(^{t}Bu$_2$bpy)$^{2+}$ was found to raise the energy level of the dithiafulvene-based π-orbital, which dramatically changed the electronic structure and caused the SOMO−HOMO energy level conversion. The resulting complex Pt(^{t}Bu$_2$bpy)(tempodt) (Chart 1) showed a unique electronic structure in which the energy level of the SOMO centered on the TEMPO moiety was lower than that of the dithiafulvene-based π-orbital (= HOMO).[1n] We also revealed that M(tempodt)$_2^{n-}$ (M = Au^{3+}, n = 1; M = Ni^{2+}, n = 2) exhibited a novel chemical reaction, an intramolecular cyclization of the TEMPO, attributable to the SOMO−HOMO converted electronic structure.[2d] These results clearly demonstrated that the construction of novel electronic structures for metalladithiolenes is a promising approach to develop new physical and chemical properties, thereby opening unexplored fields of molecular functionalities.

In the tempodt-based complexes noted above, the electronic communication between the two redox centers (the TEMPO and dithiafulvene moieties) was found to be weak due to the localized nature of the radical spin on the N−O bond in the TEMPO moiety. As a result, the molecular orbitals (MOs) of the two units overlapped poorly. The effective electronic communication between the two (or more) redox centers in these molecular systems may afford a unique electronic structure with asymmetric double-minimum potential energy curves that can be interpreted in terms of the two-state classical Marcus−Hush theory, as has been reported for a set of asymmetric mixed-valence compounds or valence tautomeric compounds.[4,5,33] If the electronic structures (potential curves) and physical properties can be controlled by external stimuli such as light, heat, or chemical environment, they are candidates for stimuli-responsible multifunctional molecular materials; Therefore, the realization of electronic communication between the dithiolene-based π-orbital and a second redox center on a metalladithiolene provides an attractive strategy for producing new types of electronic structures, leading to novel functions, such as heat-triggered nonlinear optical switching, light-induced (super)conductor-to-insulator transitions, or gigantic magnetoresistance (magneto-induced conductivity changes).

From this perspective, we developed novel ferrocenyl (Fc)-bound dithiolenes FcS$_4$dt(Me)$_2$ and FcS$_4$dt[Pt(^{t}Bu$_2$bpy)][3S] shown in Scheme 1. Ferrocene exhibits reversible redox behavior to form a paramagnetic ferrocenium ion upon oxidation, which we have employed to prepare several donor−acceptor (DA) compounds.[6] Meanwhile, one-electron

Scheme 1

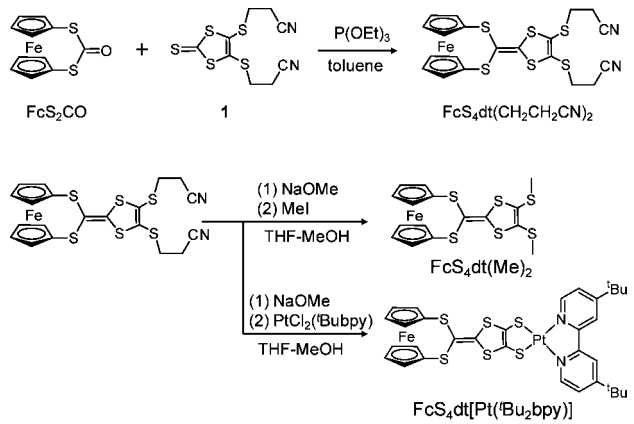

(1e$^-$) oxidation of a π-conjugated dithiolene skeleton provides π-radical electron delocalized onto the conjugated dithiolene skeleton. Several metalladithiolenes based on the ferrocene-dithiolene hybrid ligands (Chart 1) were reported, and their redox behavior and spectroscopic properties were examined; however, none of these compounds displayed electronic communication between the ferrocene and dithiolene moieties.[7] The ferrocene moiety was attached via a single bond to the dithiolene skeleton in these metalladithiolenes, which allowed for the free rotation of ferrocene relative to the dithiolene moiety, leading to negligible electronic interactions between the redox centers. In contrast, the two redox centers (a ferrocene moiety and a conjugated dithiolene) in FcS$_4$dt were closely and densely connected via two sulfur atoms with the cyclopentadienyl (Cp) rings of the ferrocene unit nearly perpendicular to the planar dithiolene skeleton. Thus, electronic communication between the two moieties was expected to proceed via efficient overlap of the MOs at the redox centers or via the electrons associated with the bridging atoms. It should be noted that the complex could potentially access a configuration in which the localized MOs (non-canonical orbitals) in the ferrocene and dithiolene moieties were orthogonal, which is important for achieving ferromagnetic spin−spin exchange interactions.

In this study, we synthesized FcS$_4$dt(Me)$_2$ and FcS$_4$dt[Pt(^{t}Bu$_2$bpy)], and their 1 e$^-$-oxidized species [FcS$_4$dt(Me)$_2$]$^{\bullet+}$ and [FcS$_4$dt[Pt(^{t}Bu$_2$bpy)]]$^{\bullet+}$. The crystal structures, physical properties, and electronic structures were investigated using single-crystal XRD analysis, cyclic voltammetry, electron paramagnetic resonance (EPR), UV−vis−NIR spectroscopy, and density functional theory (DFT) calculations. The experimental results were compared with those of related

dx.doi.org/10.1021/ic300581a | Inorg. Chem. 2012, 51, 12102−12113

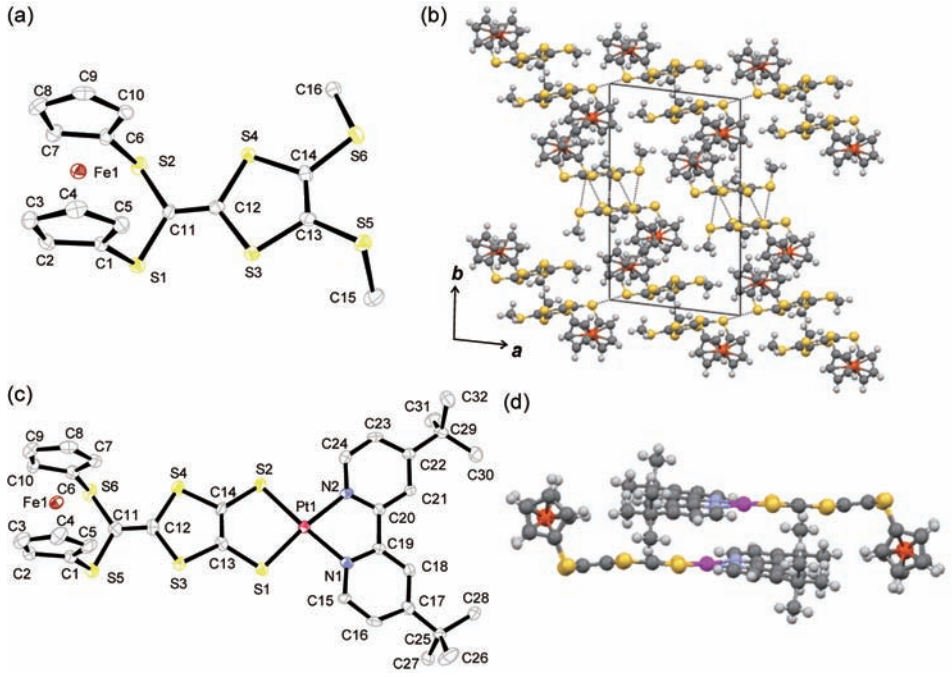

Figure 1. One of the crystallographically independent $FcS_4dt(Me)_2$ molecules with thermal ellipsoids set at 50% probability. Hydrogen atoms are omitted for clarity (a). Crystal structure of $FcS_4dt(Me)_2$ viewed along the *c*-axis. Dotted lines represent intermolecular S···S contacts (b). Molecular structure of $FcS_4dt[Pt(^tBu_2bpy)]$ with thermal ellipsoids set at 50% probability. Hydrogen atoms are omitted for clarity (c). The dimerized structure of $FcS_4dt[Pt(^tBu_2bpy)]$ in the crystal (d).

compounds, such as $chxdt(CH_2CH_2CN)_2$ and $Pt(^tBu_2bpy)$-(chxdt) (Chart 1). We succeeded in controlling the character of the HOMO of $FcS_4dt(R)_2$ and the resultant spin density distribution of $[FcS_4dt(R)_2]^{\bullet+}$ by changing R (R = Me for $FcS_4dt(Me)_2$; 2R = $Pt(^tBu_2bpy)$ for $FcS_4dt[Pt(^tBu_2bpy)]$). Significant electronic communication between the ferrocene and dithiolene moieties was detected in the oxidized species $[FcS_4dt(Me)_2]^{\bullet+}$ and $[FcS_4dt[Pt(^tBu_2bpy)]]^{\bullet+}$ as the appearance of an intramolecular charge transfer (ICT) band. Analysis of the ICT bands enabled us to elucidate the differences in their double-minimum potential energy curves and ICT directions.

RESULTS AND DISCUSSION

Synthesis and Characterization of $FcS_4dt(Me)_2$ and $FcS_4dt[Pt(^tBu_2bpy)]$. $FcS_4dt(Me)_2$ and $FcS_4dt[Pt(^tBu_2bpy)]$ were synthesized according to the procedure provided in Scheme 1.

The $P(OEt)_3$-mediated cross-coupling reaction between FcS_2CO[8] and thione 1,[9] commonly used for constructing TTF skeletons,[10] was followed by purification via silica gel column chromatography to afford $FcS_4dt(CH_2CH_2CN)_2$. The dithiolate ion, FcS_4dt^{2-}, was generated in situ by deprotecting the $-CH_2CH_2CN$ groups with NaOMe followed by reaction with MeI or $PtCl_2(^tBu_2bpy)$[11] to yield $FcS_4dt(Me)_2$ or $FcS_4dt[Pt(^tBu_2bpy)]$, respectively. The compounds were characterized and identified by NMR, ESI-TOF-MS, and elemental analysis.

Molecular Structures of the Complexes Analyzed by Single-Crystal XRD. The crystal and molecular structures of $FcS_4dt(Me)_2$ and $FcS_4dt[Pt(^tBu_2bpy)]$ were revealed by single crystal XRD measurements at 113 K. The crystal data are given in Supporting Information Table S1. Each unit cell of $FcS_4dt(Me)_2$ included two crystallographically independent $FcS_4dt(Me)_2$ molecules with similar conformations except for the orientation of the terminal $-SMe$ groups. One of the crystallographically independent $FcS_4dt(Me)_2$ molecules is shown in Figure 1a. This structure included a ferrocene moiety with two nearly parallel cyclopentadienyl rings (177°) and a conjugated planar dithiolene moiety. The two moieties were connected through the sulfur atoms S1 and S2, with C6−S2−C11 and C1−S1−C11 angles of ca. 100°. Each molecule formed a dimerized structure with overlapping planar dithiolene moieties, and the dimers were stacked in a head-to-tail manner (Figure 1b). Several short S···S distances (3.583(2)−3.681(2) Å) were observed within the dimer, which were close to the sum of the van der Waals radii of two sulfur atoms (3.6 Å). Interestingly, interdimer side-by-side S···S contacts (3.443(1) Å) were also observed. The Cp−Cp distance in ferrocene moieties (3.27 Å) was comparable to the distance between the sulfur atoms S1 and S2 (3.067 Å) or S3 and S4 (2.956 Å), indicating that the introduction of the ferrocene moiety did not disturb the intermolecular side-by-side interactions through the sulfur atoms.

The molecular structure of $FcS_4dt[Pt(^tBu_2bpy)]$ is shown in Figure 1c. One crystallographically independent $FcS_4dt[Pt(^tBu_2bpy)]$ molecule was present in the crystal lattice. The ferrocene and conjugated platinadithiolene moieties were connected through the sulfur atoms S5 and S6, with C6−S6−C11 and C1−S5−C11 angles of ca. 101°, similar to those of $FcS_4dt(Me)_2$. The central Pt atom formed a slightly distorted square-planar geometry with a tilt angle of 6.9° between the Pt1S1C13C14S2 plane and the Pt1N1C19C20N2 plane, in contrast with the almost perfect planar coordination environment around Pt in $Pt(^tBu_2bpy)$(tempodt) and $Pt(^tBu_2bpy)$-(chxdt).[1n,13] $FcS_4dt[Pt(^tBu_2bpy)]$ molecules formed a head-to-tail dimer in the solid state (Figure 1d), in which an electron-accepting bpy skeleton and an electron-donating conjugated platinadithiolene skeleton faced one another, as has been

dx.doi.org/10.1021/ic300581a | *Inorg. Chem.* 2012, 51, 12102−12113

observed in single crystals of Pt(^{t}Bu$_2$bpy)(chxdt).[13] The interplane distance within a dimer was ca. 3.4 Å, suggesting the presence of $\pi-\pi$ interactions within the dimer complexes. Close interdimer $C_{Cp}\cdots C_{Cp}$ distances (3.34(1) Å) were also observed.

The bridging mode of the two redox centers (the ferrocene and dithiolene moieties) in the two complexes, in which the conjugated dithiolene and Cp planes in the ferrocene moiety were perpendicular, was distinct from that for reported ferrocene–metalladithiolenes (Chart 1). Previous reports of the ferrocene–dithiolene or ferrocene–metalladithiolene hybrid molecules,[7,14] in which the ferrocene moiety was connected to a dithiolene (TTF) moiety in a flexible manner via a single bond, indicated that the bulkiness of the ferrocene moiety could disturb the intermolecular face-to-face or side-by-side interactions between dithiolene moieties in the solid state. In contrast, the orientationally constrained binding of the ferrocene moiety to the planar dithiolene skeleton via two sulfur atoms in the FcS_4dt molecular system facilitated efficient intermolecular interactions via $\pi-\pi$ stacking and side-by-side S···S contacts, in addition to Cp–Cp contacts.[12]

Electrochemistry of the Complexes. The electrochemical properties of $FcS_4dt(Me)_2$ and $FcS_4dt[Pt(^tBu_2bpy)]$ were investigated by cyclic voltammetry in an effort to elucidate the electronic structures around the frontier orbitals. Figure 2a

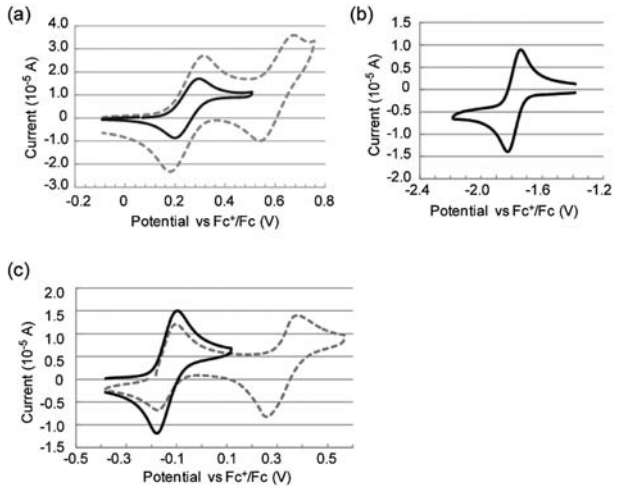

Figure 2. Cyclic voltammograms of $FcS_4dt(Me)_2$ at 30 (plain line) and at 100 mV/s (dashed line) (a) and those of $FcS_4dt[Pt(^tBu_2bpy)]$ at 100 mV/s for reduction (b) and for oxidation (c) in 0.1 M $Bu_4N{\cdot}ClO_4$–CH_2Cl_2 at r.t.

displays the cyclic voltammograms of $FcS_4dt(Me)_2$ in CH_2Cl_2, measured at room temperature. $FcS_2dt(Me)_2$ displayed a reversible oxidation wave ($E_1^{0\prime ox}$ = 0.26 V vs ferrocenium/ferrocene) and a quasi-reversible one[32] at more positive potential ($E_2^{0\prime ox} \approx 0.60$ V), in accordance with the fact that $FcS_4dt(Me)_2$ has two electron-donating ferrocene and π-conjugated dithiolene moieties. These reduction potentials were compared with those of related compounds in Table 1 to identify the reaction center involved in each oxidation step. Interestingly, the first reduction potential $E_1^{0\prime ox}$ for $FcS_4dt(Me)_2$ was intermediate between the reduction potentials of the reference complexes FcS_2CH_2[15] and chxdt$(CH_2CH_2CN)_2$.[1n] Thus, it was difficult to identify the moiety from which an electron was removed during the first 1 e$^-$ oxidation process. The first oxidation process appeared to be ferrocene-centered,

Table 1. Redox Potentials[a] of $FcS_4dt(Me)_2$, $FcS_4dt[Pt(^tBu_2bpy)]$, and Related Compounds

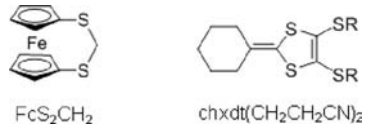

compound	$E_1^{0\prime red}$	$E_1^{0\prime ox}$	$E_2^{0\prime ox}$
$FcS_4dt(Me)_2$		0.26	
FcS_2CH_2[b]		0.22	0.60
chxdt$(CH_2CH_2CN)_2$		0.36[c]	
$FcS_4dt[Pt(^tBu_2bpy)]$	−1.78	−0.14	0.33
$Pt(^tBu_2bpy)$(chxdt)	−1.76	−0.24	

[a]Versus ferrocenium/ferrocene in 0.1 M Bu_4NClO_4–CH_2Cl_2. [b]In 0.1 M Bu_4NClO_4–CH_3CN. [c]Anodic peak potential.

based on the combined analysis of UV–vis–NIR, EPR, and DFT results, as described below. The second oxidation was thus ascribed to the conjugated dithiolene moiety. Interestingly, the reduction potential $E_2^{0\prime ox}$ was 0.60 V, much more positive than $E_2^{0\prime ox}$ of chxdt$(CH_2CH_2CN)_2$. This result indicated that the 1 e$^-$-oxidized state was stabilized by electronic communication between the ferrocene and dithiolene moieties, as has been observed in class II mixed valence compounds. This observation was consistent with the results of EPR and UV–vis–NIR spectra, as mentioned below. It should be noted that electrostatic interactions also contributed to the positive $E_2^{0\prime ox}$ value, in which the positive charge on the ferrocene moiety influenced the second oxidation process on the dithiolene skeleton.[34]

Cyclic voltammetry of $FcS_4dt[Pt(^tBu_2bpy)]$ in CH_2Cl_2 at room temperature demonstrated one reversible reduction wave ($E_1^{0\prime red}$ = −1.78 V vs ferrocenium/ferrocene), one reversible oxidation wave ($E_1^{0\prime ox}$ = −0.14 V) and one quasi-reversible wave[32] ($E_2^{0\prime ox} \approx 0.33$ V), as shown in Figure 2b and c and Table 1. The reduction process was attributed to the LUMO based on the Pt-bpy moiety, as in $Pt(^tBu_2bpy)$(chxdt)[1n] and other Pt(diimine)(dithiolate) complexes.[1h–j,36] The two oxidation waves were derived from the electron-donating ferrocene and conjugated platinadithiolene moieties. $E_1^{0\prime ox}$ was much more negative than the corresponding values for $FcS_4dt(Me)_2$ and FcS_2CH_2, although it was close to the value for $Pt(^tBu_2bpy)$(chxdt). This observation suggested that the first oxidation of $FcS_4dt[Pt(^tBu_2bpy)]$ was centered at the platinadithiolene moiety. The second oxidation process could be ascribed to the ferrocene moiety. These results indicated that the HOMO of $FcS_4dt[Pt(^tBu_2bpy)]$ was centered on the conjugated platinadithiolene unit, in sharp contrast to $FcS_4dt(Me)_2$, in which the HOMO was located at the ferrocene moiety. Such differences in the electronic structures around the HOMO levels of the two compounds were expected, considering the relative energy difference between the ferrocene-based orbital and the conjugated dithiolene-based orbital. The dithiolene-centered π-orbital on the FcS_4dt skeleton was destabilized by ligation to $Pt(^tBu_2bpy)^{2+}$, which raised the energy level of the dithiolene-centered π-orbital of the resulting $FcS_4dt[Pt(^tBu_2bpy)]$ above the energy level of the ferrocene-centered orbital (Figure 6). A similar energetic situation was observed for $Pt(^tBu_2bpy)$(tempodt), in which the ligation of tempodt to $Pt(^tBu_2bpy)^{2+}$ destabilized the dithiolene-based orbital to cause SOMO–HOMO conversion.[1n] We note that $E_2^{0\prime ox}$ for $FcS_4dt[Pt(^tBu_2bpy)]$ was more positive than $E_1^{0\prime ox}$ for FcS_2CH_2 and

dx.doi.org/10.1021/ic300581a | Inorg. Chem. 2012, 51, 12102–12113

$E_1^{0\prime ox}$ for $FcS_4dt(Me)_2$, suggesting that electronic and electrostatic interactions between the two redox centers were operative in the 1 e^--oxidized state. An additional small oxidation wave was detected above 0.60 V, suggesting further oxidation of $[FcS_4dt[Pt(^tBu_2bpy)]]^{2+}$ (Supporting Information Figure S1). This feature was not examined further in this study.

EPR Study of the Complexes upon Oxidation. The EPR spectra of the 1 e^--oxidized compounds, $[FcS_4dt(Me)_2]^{\bullet+}$ and $[FcS_4dt[Pt(^tBu_2bpy)]]^{\bullet+}$, were measured in an effort to elucidate the redox center involved in the first oxidation process. One-electron oxidation of the samples in CH_2Cl_2 was carried out chemically using tris(4-bromophenyl)ammoniumyl hexachloroantimonate as the oxidant. The generated $[FcS_4dt(Me)_2]^{\bullet+}$ was thermally unstable and decomposed gradually above 0 °C; thus, the oxidation reaction was conducted at −78 °C. In contrast, $[FcS_4dt[Pt(^tBu_2bpy)]]^{\bullet+}$ was stable in CH_2Cl_2, even at room temperature under a nitrogen atmosphere.

The EPR spectrum of $[FcS_4dt(Me)_2]^{\bullet+}$ in CH_2Cl_2 (0.26 mM), measured at 7.5 K, is depicted in Figure 3. A highly

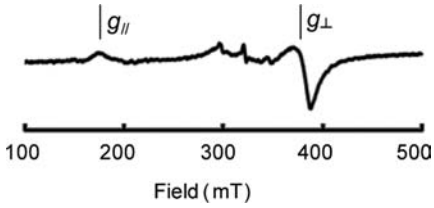

Figure 3. EPR spectrum of $[FcS_4dt(Me)_2]^{\bullet+}$ in frozen CH_2Cl_2 measured at 7.5 K. $g_{\|}$ = 3.70, $g_\perp$ = 1.70.

anisotropic EPR signal with an axial character was observed at $g_{\|}$ = 3.70 and $g_\perp$ = 1.70 only below 20 K. The anisotropy and the obtained parameters were characteristic of ferrocenium derivatives (Table 2),[16] suggesting that the spin density was

Table 2. *g* Values of the Ferrocenium Derivatives[16]

compound	$g_{\|}$	$g_\perp$
$[Fe(C_5H_5)_2]^+$	4.35	1.26
$[Fe(C_5H_5)(C_5H_4\text{-}Me)]^+$	4.17	1.47
$[Fe(C_5H_4\text{-}Me)_2]^+$	3.83	1.67
$[FcS_4dt(Me)_2]^+$	3.70	1.70

effectively localized over the Fe atom in the ferrocene moiety. The anisotropy of the obtained *g*-values was smaller (the *g*-values were closer to 2.00) than those of ferrocenium ion and its derivatives, indicating that the spin density extended over the conjugated dithiolene skeleton. These results suggested that the HOMO of $FcS_4dt(Me)_2$ was localized mainly over the ferrocene moiety, with some density over the π−conjugated dithiolene plane, in good agreement with the CV results and the HOMO calculated by DFT methods, discussed below. The small signals observed at 300−340 mT originated from decomposed species. The intensities of these signals increased and the signals from $[FcS_4dt(Me)_2]^{\bullet+}$ decreased upon warming to 293 K, which resulted in the partial decomposition of $[FcS_4dt(Me)_2]^{\bullet+}$, followed by cooling to 8.3 K (Supporting Information Figure S2).

The CH_2Cl_2 solution of $[FcS_4dt[Pt(^tBu_2bpy)]]^{\bullet+}$ did not show an EPR signal at any temperature, as was observed for the reference compound $[Pt(^tBu_2bpy)(chxdt)]^{\bullet+}$. This might be resulted from the weak π-dimer formation in the solution, in which through-space antiferromagnetic interaction leads to the singlet spin state. It should be noted that the $[FcS_4dt[Pt(^tBu_2bpy)]]^{\bullet+}$ cations formed weak π-dimer in the crystal lattice as mentioned below (Figure 10) and that a powder sample of $[FcS_4dt[Pt(^tBu_2bpy)]](F4TCNQ)\cdot C_6H_{14}\cdot CH_2Cl_2$ displayed no EPR signals derived from $[FcS_4dt[Pt(^tBu_2bpy)]]^{\bullet+}$. These results support that the π-dimerization is plausible in the solution.

UV−vis Spectroscopy and the Calculated Electronic Structures of the Complexes. The electronic structures of the compounds $FcS_4dt(Me)_2$ and $FcS_4dt[Pt(^tBu_2bpy)]$ were investigated by means of UV−vis spectroscopy, in combination with DFT calculations. As shown in Figure 4a, $FcS_4dt(Me)_2$

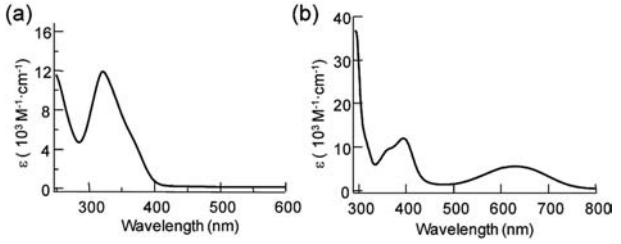

Figure 4. UV−vis spectra in CH_2Cl_2 of $FcS_4dt(Me)_2$ (a) and of $FcS_4dt[Pt(^tBu_2bpy)]$ (b).

displayed absorption bands at 322 (ε = 11800 M^{-1} cm^{-1}), 374 (4500 M^{-1} cm^{-1}), and 450 nm (<200 M^{-1} cm^{-1}). The two former absorptions with high ε values were assigned to the conjugated dithiolene-based $\pi-\pi^*$ transition. The latter absorption band was assigned to a symmetry-forbidden d−d transition centered on the ferrocene moiety by comparison with the spectra of chxdt and ferrocene.

$FcS_4dt[Pt(^tBu_2bpy)]$ displayed characteristic absorptions at 360 (ε = 9730 M^{-1} cm^{-1}), 393 (11 700 M^{-1} cm^{-1}), and 630 nm (5470 M^{-1} cm^{-1}) similar to those of the reference complex $Pt(^tBu_2bpy)(chxdt)$ (Figure 4b).[1n] The lowest energy absorption was assigned to an intramolecular charge transfer band (the mixed metal−ligand to ligand charge transfer band, MMLL′CT band) from the conjugated metalladithiolene moiety (HOMO) to the bpy moiety (LUMO). Such features are commonly observed for Pt(diimine)(dithiolate) complexes.[1h−j,36]

The spectroscopic results, combined with the electrochemical and EPR results for $FcS_4dt(Me)_2$ and $FcS_4dt[Pt(^tBu_2bpy)]$, could be interpreted by the calculated electronic structures based on the DFT methods. Figure 5 shows the electronic structure of $FcS_4dt(Me)_2$, calculated at the BP86/def2-SVP level of theory. The frontier orbitals of the reference compound $chxdt(Me)_2$ are shown for comparison. The LUMO of $FcS_4dt(Me)_2$ (117) was similar to that of $chxdt(Me)_2$, whereas the MOs of the dithiolene moiety and the ferrocene moiety were well-hybridized to construct the HOMO (116), HOMO-1 (115), and HOMO-3 (113). This energetic situation is illustrated in Figure 6a. Because the energy level of the HOMOs of FcS_2CH_2 and $chxdt(Me)_2$ were comparable, as indicated by the similarities between their first reduction potentials ($E_1^{0\prime ox}$ in Table 1), electronic interactions through overlap of the ferrocene-based and dithiolene-based MOs, mediated by the bridging sulfur atoms, produced hybridized MOs in $FcS_4dt(Me)_2$. The bonding and antibonding combination between the HOMOs of FcS_2CH_2 and $chxdt(Me)_2$ afforded the HOMO and HOMO-3 of $FcS_4dt(Me)_2$, respectively. The HOMO was localized at the ferrocene moiety

dx.doi.org/10.1021/ic300581a | *Inorg. Chem.* 2012, 51, 12102−12113

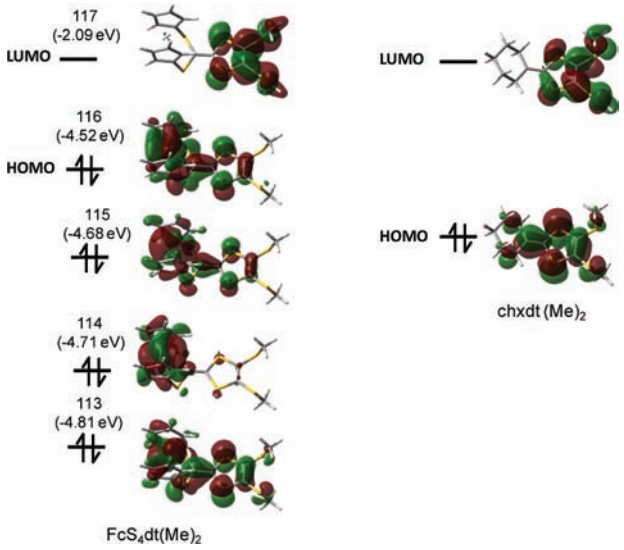

Figure 5. Calculated MOs for $FcS_4dt(Me)_2$ and $chxdt(Me)_2$.

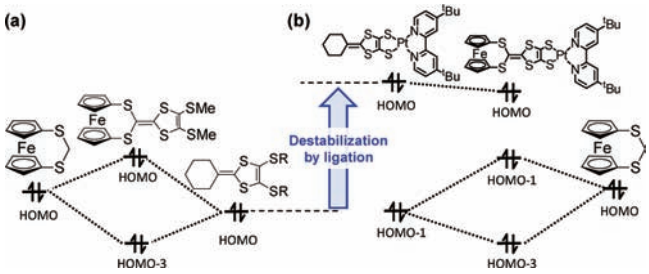

Figure 6. Schematic representation of the interactions of the orbitals in (a) $FcS_4dt(Me)_2$ and (b) $FcS_4dt[Pt(^tBu_2bpy)]$.

with extension onto the π-conjugated dithiolene skeleton. The ferrocene-based nature of the HOMO was revealed by EPR spectroscopy of $[FcS_4dt(Me)_2]^{\bullet+}$, as discussed above. Time-dependent(TD)-DFT calculations reproduced the observed UV–vis spectrum (Supporting Information Table S2), and the assignment of electronic transitions was consistent with the experimental studies mentioned above.

The MOs calculated for $FcS_4dt[Pt(^tBu_2bpy)]$ at the B3LYP/LANL2DZ (Fe and Pt atom) and/6-31G(d) (all other atoms) levels of theory are shown in Figure 7a. The frontier orbitals were almost identical to those of the reference compound $Pt(^tBu_2bpy)(chxdt)$, in which the HOMO (184) was mainly centered over the π-conjugated dithiolene backbone with a minor contribution from the Pt atom and a negligible contribution from the Fe atom. The LUMO (185) was centered at the bpy moiety. The MOs around the HOMO to HOMO-3 (181) for $FcS_4dt[Pt(^tBu_2bpy)]$ could be rationalized as shown in Figure 6b. The energy level of the dithiolene-based π-orbital (the HOMO of $Pt(^tBu_2bpy)(chxdt)$) was much higher in energy than that of FcS_2CH_2, as indicated by CV (Table 1), so that the interaction between the π-conjugated dithiolene and ferrocene moieties was considerably weak for $FcS_4dt[Pt(^tBu_2bpy)]$. The ligation of FcS_4dt to $Pt(^tBu_2bpy)^{2+}$ raised the energy level of the conjugated dithiolene-based orbital, thereby producing a dithiolene-based HOMO with high energy. This situation contrasted sharply with the electronic structure of $FcS_4dt(Me)_2$, where the near identical energy levels of the two moieties yield hybridized MOs (Figure 5). The bonding and antibonding combinations between the HOMO-1 of

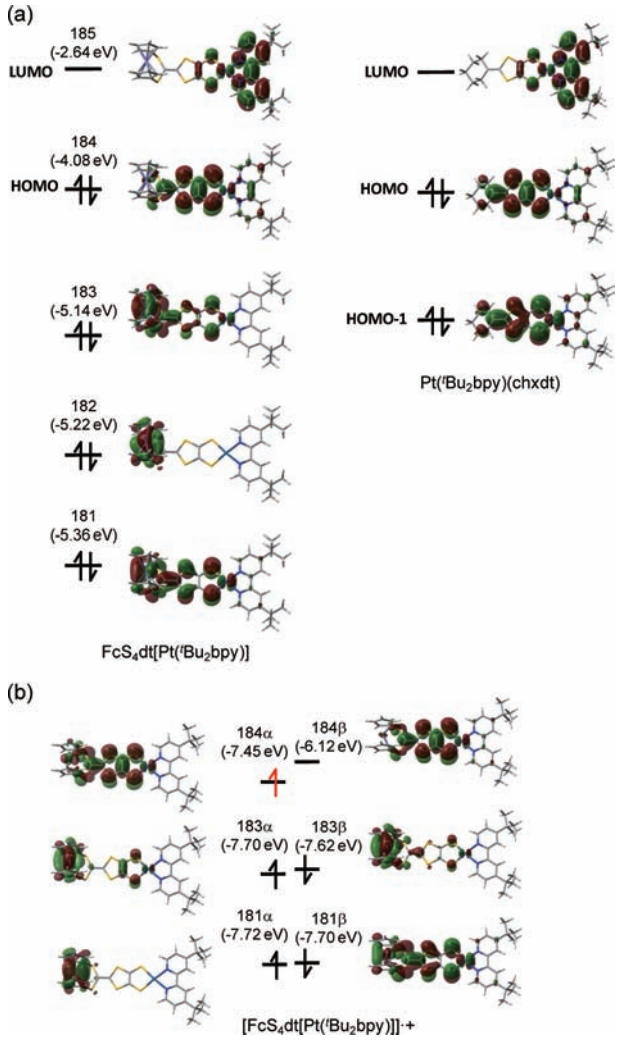

Figure 7. Calculated MOs for $FcS_4dt[Pt(^tBu_2bpy)]$ and $Pt(^tBu_2bpy)$-(chxdt) (a) and those for $[FcS_4dt[Pt(^tBu_2bpy)]]^{\bullet+}$ (b).

$Pt(^tBu_2bpy)(chxdt)$ and the HOMO of FcS_2CH_2 gave the hybridized MOs HOMO-1 (183) and HOMO-3 (181), respectively. The electronic transitions observed in the UV–vis spectrum were again reproduced by the TD-DFT calculation (Supporting Information Table S3). It is of quite importance that the character of the HOMOs of $FcS_4dt(Me)_2$ and $FcS_4dt[Pt(^tBu_2bpy)]$ showed clear differences, which was caused by changing the relative energy levels between the two redox centers.

Vis–NIR Spectroscopy of the Complexes under 1 e^- Oxidation. We next focus on the Vis–NIR spectroscopic studies of the 1 e^--oxidized cation radicals $[FcS_4dt(Me)_2]^{\bullet+}$ and $[FcS_4dt[Pt(^tBu_2bpy)]]^{\bullet+}$ in order to investigate the electronic communication between the ferrocene and conjugated dithiolene moieties. Electronic communication would be evidenced by the presence of ICT or intervalence charge transfer (IVCT) absorption bands, as observed for DA compounds or mixed-valence complexes. Analysis of the bands enabled us to estimate the degree of electronic communication and characterize the unique electronic structure.[4,5]

The Vis–NIR absorption spectrum of a dichloromethane solution of $[FcS_4dt(Me)_2]^{\bullet+}$ prepared in situ using tris(4-bromophenyl)ammoniumyl hexachloroantimonate as the oxi-

dx.doi.org/10.1021/ic300581a | Inorg. Chem. 2012, 51, 12102–12113

dant at 233 K represented two bands in the NIR region at 834 (ε = 60 M^{-1} cm^{-1}) and 1640 nm (217 M^{-1} cm^{-1}), as shown in Figure 8a. The intensity and spectral shape of the former was

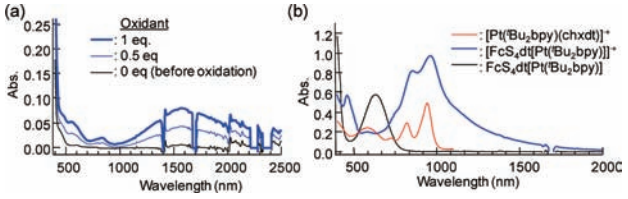

Figure 8. Vis−NIR spectra of $FcS_4dt(Me)_2$ upon 1 e^- oxidation: (black line) $FcS_4dt(Me)_2$, (blue line) addition of 0.5 equiv of the oxidant, (blue bold line) addition of 1 equiv of the oxidant (= $[FcS_4dt(Me)_2]^{\bullet+}$) (a). Vis−NIR spectra of $FcS_4dt[Pt(^tBu_2bpy)]$ (black line) and $[FcS_4dt[Pt(^tBu_2bpy)]]^{\bullet+}$ (blue line). The spectrum of $[Pt(^tBu_2bpy)(chxdt)]^{\bullet+}$ is shown for comparison (red line) (b).

similar to that of ferrocenium ion, suggesting that this absorption was ferrocenium-centered. This assignment did not conflict with the EPR results for $[FcS_4dt(Me)_2]^{\bullet+}$. On the other hand, the latter absorption was quite broad, extending over 2500 nm. An absorption band with these characteristics was not observed for ferrocene or the reference compound chxdt under 1 e^- oxidation; therefore, the band was assigned to the ICT transition. In this case, the conjugated dithiolene skeleton functioned as an electron donor, whereas the ferrocenium moiety acted as an electron acceptor. The spectra clearly indicated the electronic communication between the two moieties, which was nearly undetectable in other ferrocene−dithiolene hybrid molecules.[18] This ICT transition allowed the electronic structure change from a ferrocenium$^+$−dithiolene state (ground state for $[FcS_4dt(Me)_2]^{\bullet+}$) to a ferrocene−dithiolene$^+$ state (low-lying excited state) accompanying the electron transfer from the dithiolene skeleton to the ferrocene moiety.

Figure 8b displays the vis−NIR absorption spectra of $[FcS_4dt[Pt(^tBu_2bpy)]]^{\bullet+}$ and its reference compound $[Pt(^tBu_2bpy)(chxdt)]^{\bullet+}$. Similar spectral features were detected: $[FcS_4dt[Pt(^tBu_2bpy)]]^{\bullet+}$ showed strong absorptions at 968 and 852 nm, together with a shoulder at 754 nm, whereas $[Pt(^tBu_2bpy)(chxdt)]^{\bullet+}$ displayed strong absorption bands at 940, 820, and 732 nm. The similarities indicated that the compounds had similar electronic structures in the frontier orbital region. We revealed previously in a study of $[Pt(^tBu_2bpy)(chxdt)]^{\bullet+}$ that the oxidation of $Pt(^tBu_2bpy)(chxdt)$ removed an electron from the conjugated dithiolene moiety to form a dithiolene-based π-radical.[1n] The observed bands were then assigned to a dithiolene-based $\pi-\pi^*$ transition. This result strongly suggested that the oxidation reaction occurred on the conjugated dithiolene skeleton, supporting the assertion that the HOMO of $FcS_4dt[Pt(^tBu_2bpy)]$ was centered not over the ferrocene moiety, but rather over the conjugated dithiolene moiety.

Interestingly, a broad absorption tail extending to 2000 nm was observed in $[FcS_4dt[Pt(^tBu_2bpy)]]^{\bullet+}$ but not in $[Pt(^tBu_2bpy)(chxdt)]^{\bullet+}$. The spectra were deconvoluted to characterize the broad absorption band, which overlapped with the above-mentioned $\pi-\pi^*$ transition bands (Supporting Information Figure S3). This absorption was ascribed to an ICT transition. This result demonstrated the presence of significant electronic communication between the two moieties, in which the ferrocene moiety functioned as an electron donor and the oxidized dithiolene moiety acted as an electron acceptor. The ICT transition induced an electronic structural transition from the ferrocene−dithiolene$^+$ state (ground state for $[FcS_4dt[Pt(^tBu_2bpy)]]^{\bullet+}$) to the ferrocenium$^+$−dithiolene state (low-lying excited state), accompanying the electron transfer from the ferrocene unit to the dithiolene moiety. The direction of ICT was reversed between $[FcS_4dt(Me)_2]^{\bullet+}$ and $[FcS_4dt[Pt(^tBu_2bpy)]]^{\bullet+}$). These explanations were consistent with the electronic structures and transition energies of $[FcS_4dt[Pt(^tBu_2bpy)]]^{\bullet+}$, calculated using DFT and TD-DFT methods. As shown in Figure 7b, the singly occupied molecular orbital (SOMO) of $[FcS_4dt[Pt(^tBu_2bpy)]]^{\bullet+}$ was delocalized over the dithiolene skeleton with little participation of the ferrocene moiety, consistent with the vis−NIR results. TD-DFT calculations predicted the presence of electronic transitions at 1087 and 876 nm (Supporting Information Table S4). The former 183β−184β transition corresponded to an ICT from the ferrocene to dithiolene moieties (Figure 7b) and, therefore, corresponded to the broad absorption band in Figure 8b. The latter 182β−184β transition indicated a $\pi-\pi^*$ transition centered at the conjugated dithiolene moiety and corresponded to the absorption bands observed over the range 700−1000 nm. Interestingly, the observed $\pi-\pi^*$ transitions showed three distinct peaks at 968, 852, 754 nm. Similar characteristics were observed in the reference complex $[Pt(^tBu_2bpy)(chxdt)]^{\bullet+}$, which displayed three peaks in the vis−NIR spectrum (Figure 8b), although a single $\pi-\pi^*$ transition at 819 nm was predicted by the TD-DFT calculations. The three peaks presumably originated from vibronic coupling or π-dimer formation in solution.

Estimation of the Electronic Coupling Parameters and the Potential Energy Curve. ICT (IVCT) transitions have been used as sensitive probes of electron transfer processes in DA compounds and class II mixed-valence complexes. The energy (ν_{max}), intensity (ε_{max}), and bandwidth at the half-height ($\Delta\nu_{1/2}$) of an ICT band are related to the electronic coupling parameter H_{AB} by eq 1.[4,5] H_{AB} indicates the degree of electronic communication between two interacting redox centers. r_{DA} in eq 1 is the distance between D and A, commonly estimated from crystallographic data. In our case, for $[FcS_4dt(Me)_2]^{\bullet+}$, the ferrocenium moiety behaved as A and the dithiolene moiety behaved as D, whereas the ferrocene moiety behaved as D and the cationic platinadithiolene moiety behaved as A for $[FcS_4dt[Pt(^tBu_2bpy)]]^{\bullet+}$. Thus, it was possible to estimate H_{AB} for $[FcS_4dt(Me)_2]^{\bullet+}$ and $[FcS_4dt[Pt(^tBu_2bpy)]]^{\bullet+}$ by analyzing the ICT bands. The extracted spectral parameters are presented in Table 3. We defined r_{DA} as the distance between Fe atom and the center of the C−S−C−C−S ring (see the caption in Table 3), although the accurate estimation of r_{DA} was difficult because of the wide delocalization of the π-orbital across the dithiolene moiety. H_{AB} for $[FcS_4dt(Me)_2]^{\bullet+}$ was moderate (429 cm^{-1}), comparable to that of a ferrocene−polychlorotriphenylmethyl radical-based DA compound constructing an asymmetric double-minimum potential energy curve.[4b] The value of H_{AB} for $[FcS_4dt[Pt(^tBu_2bpy)]]^{\bullet+}$ was larger than that for $[FcS_4dt(Me)_2]^{\bullet+}$. This indicated that the electronic coupling strength could be dramatically modulated by substituting R in $FcS_4dt(R)_2$ (R = Me for $FcS_4dt(Me)_2$; 2R = $Pt(^tBu_2bpy)$ for $FcS_4dt[Pt(^tBu_2bpy)]$).

The obtained parameters, listed in Table 3, enabled us to estimate the electronic potential energy curves of the complexes based on the two-state classical Marcus−Hush theory.[4,5] As depicted in Figure 9a, two diabatic potential curves (the energy

dx.doi.org/10.1021/ic300581a | Inorg. Chem. 2012, 51, 12102−12113

Table 3. Spectral Data for the ICT Bands

	$[FcS_4dt(Me)_2]^{\bullet+}$	$[FcS_4dt[Pt(^tBu_2bpy)]]^{\bullet+a}$
υ_{max} (cm^{-1})	6350	10700
ε_{max} (M^{-1} cm^{-1})	217	5460
$\Delta\upsilon_{1/2}$ (cm^{-1})	4240	5000
H_{AB} (cm^{-1})	429	3302
r_{DA} (Å)	3.37[b]	3.37[c]
ΔG^0 (cm^{-1})	887[d]	3710[e]

[a]ICT band and its parameters were extracted by deconvolution of the observed NIR spectrum (Supporting Information Figure S3). [b]The distance between the Fe atom and the center of the C12−S3−C13−C14−S4 ring for $FcS_4dt(Me)_2$, revealed by single-crystal XRD studies. [c]The distance between the Fe atom and the center of the C12−S3−C13−C14−S4 ring for $FcS_4dt[Pt(^tBu_2bpy)]$, revealed by single crystal XRD analysis. [d]The differences in the anodic peak potentials of FcS_2CH_2 and $chxdt(CH_2CH_2CN)_2$, shown in Table 2. [e]The differences in the first reduction potentials E_1^{ox} or FcS_2CH_2 and $Pt(^tBu_2bpy)(chxdt)$, shown in Table 2.

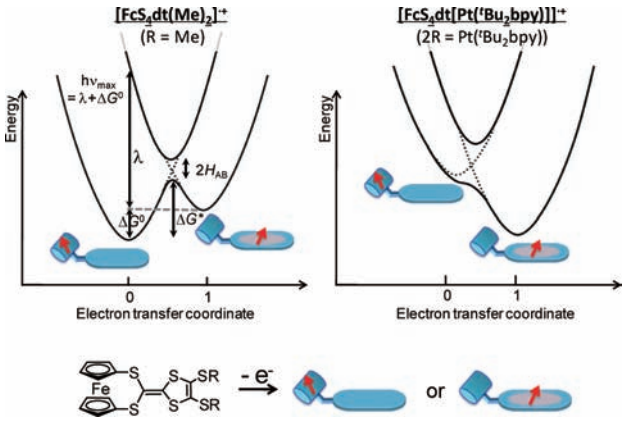

Figure 9. Adiabatic (black line) and diabatic (dashed line) potential energy surfaces as a function of the electron transfer coordinates of $[FcS_4dt(Me)_2]^{\bullet+}$ and $[FcS_4dt[Pt(^tBu_2bpy)]]^{\bullet+}$ estimated from the parameters given in Table 3.

curves for the ground and ICT states), described as λX^2 and $\lambda(X-1)^2$, were used to construct an adiabatic potential energy curve through H_{AB}. X is the electron transfer coordinate, and λ is the reorganization energy given by eq 2. ΔG^0 is approximately treated as the difference between the oxidation (or reduction) potentials at the two redox centers.

$$H_{ab} = 0.0206(\upsilon_{max}\varepsilon_{max}\Delta\upsilon_{1/2})^{1/2}/r_{DA} \quad (1)$$

$$\lambda = h\upsilon_{max} - \Delta G^0 \quad (2)$$

The potential energy curves calculated for $[FcS_4dt(Me)_2]^{\bullet+}$ and $[FcS_4dt[Pt(^tBu_2bpy)]]^{\bullet+}$ are illustrated in Figure 9a and b, respectively. The curves clearly differed. Although some approximations were introduced into the calculation to obtain these energy curves, the curves provide a model for the obtained experimental results (CV, EPR, vis−NIR) and the (TD-)DFT calculations. The electronic communication strength (H_{AB}), ICT direction, and electronic structure (MOs and potential energy curves) of FcS_4dt-based complexes could be controlled by changing the energy level of the dithiolene-based MOs.

Determination of the Crystal Structure of the $[FcS_4dt[Pt(^tBu_2bpy)]]^{\bullet+}$ Cation Radical Salt by Single-Crystal XRD Analysis. Attempts have been made to prepare single crystals of the $[FcS_4dt[Pt(^tBu_2bpy)]]^{\bullet+}$ cation radical in an effort to characterize its electronic structure from a structural point of view. Crystallization of the cation radical proved to be challenging because Pt(diimine)(dithiolate) complexes decompose or display a monomer−dimer equilibrium[17] upon oxidation, which could make the isolation of [Pt(diimine)-(dithiolate)]$^+$ species difficult. Only two examples of the successful crystal structure analysis of [Pt(diimine)-(dithiolate)]$^+$ cation salt have been reported. Pap et al. described the crystal structure of $[Pt(^tBu_2bpy)(A)]_2(PF_6)_2{\cdot}3CH_2Cl_2$ (A^{2-} = 1,2-bis(4-tert-butylphenyl)-ethylene-1,2-dithiolate) in which the cations formed a σ-dimer through Pt−S bonding.[17c] Meanwhile, the cation was present in a monomeric state in the crystal of $[Pt(bpy)(B)](BF_4)$ (bpy =2,2′-bipyridine; B^{2-} = 2-{(4,5-ethylenedithio)-1,3-dithiole-2-ylidene}-1,3-dithiole-4,5-dithionate), as reported by Kubo and co-workers.[29] $FcS_4dt[Pt(^tBu_2bpy)]$ was chemically oxidized using a series of oxidants then crystallized in the presence of a variety of counteranions, including PF_6^-, BF_4^-. Finally, we succeeded in obtaining single crystals of $[FcS_4dt-[Pt(^tBu_2bpy)]](F4TCNQ){\cdot}(C_6H_{14}){\cdot}(CH_2Cl_2)$ using F_4TCNQ as an oxidant. The monoanionic character of $(F_4TCNQ)^-$ anions in the crystal was revealed by IR spectroscopy,[19] which also provided evidence in support of the monocationic nature of $[FcS_4dt[Pt(^tBu_2bpy)]]^{\bullet+}$ with the 1:1 molar ratio of $FcS_4dt[Pt(^tBu_2bpy)]$:F_4TCNQ in the crystal.

The crystal $[FcS_4dt[Pt(^tBu_2bpy)]]-(F_4TCNQ){\cdot}C_6H_{14}{\cdot}CH_2Cl_2$ contained one crystallographically independent $[FcS_4dt[Pt(^tBu_2bpy)]]^{\bullet+}$ cation, two halves of the $(F_4TCNQ)^-$ anions (A and B), one hexane, and one dichloromethane. The dichloromethane molecule was disordered at two sites with the occupancies of 0.52:0.48. Both anions A and B were planar with bond lengths and angles similar to those of the previously reported $(F_4TCNQ)^-$ ion,[30] supporting their monoanionic nature. The $[FcS_4dt[Pt-(^tBu_2bpy)]]^{\bullet+}$ ion adopted a square-planar coordination geometry around the Pt atom, in which the conjugated dithiolene and bipyridine moieties were fairly planar (Figure 10a). The cations formed a π-dimer structure in the lattice, and the cation π-dimer C−C and anion A formed a 1D $\pi-\pi$ stacking structure along the a-axis with a −C−C−A−C−C−A− configuration, as shown in Figure 10b. The anion B was relatively isolated and was surrounded by the cations and the solvent molecules (Figure 10c). Upon oxidation, the ferrocene derivatives induce a tilt in the two Cp rings with an angle of ca. 10°,[20] and metalladithiolenes show characteristic bond elongation/reduction reflecting their HOMOs.[1f,21] Thus, a comparison of the structural parameters of the $[FcS_4dt[Pt-(^tBu_2bpy)]]^{\bullet+}$ ion and the neutral $FcS_4dt[Pt(^tBu_2bpy)]$ will provide valuable information about the oxidation center of $FcS_4dt[Pt(^tBu_2bpy)]$. The atomic distances and angles between the two Cp rings in $[FcS_4dt[Pt(^tBu_2bpy)]]^{\bullet+}$ were similar to those of the neutral $FcS_4dt[Pt(^tBu_2bpy)]$; however, clear differences in the atomic distances of the two dithiolene skeletons were observed (Table 4), despite the moderate accuracy of the bond lengths of $[FcS_4dt[Pt(^tBu_2bpy)]]^{\bullet+}$. The C−C bond **d** was elongated and the C−S bond **e** was reduced by oxidation. These structural tendencies were consistent with the calculated bond lengths (Table 4) and could be interpreted in terms of the electron density distribution of the HOMO of $FcS_4dt[Pt(^tBu_2bpy)]$ (Figure 7a), in which bonds **d** and **e** have bonding and antibonding characters, respectively. These results undoubtedly suggest that the 1 e^- oxidation of $FcS_4dt[Pt-$

dx.doi.org/10.1021/ic300581a | Inorg. Chem. 2012, 51, 12102−12113

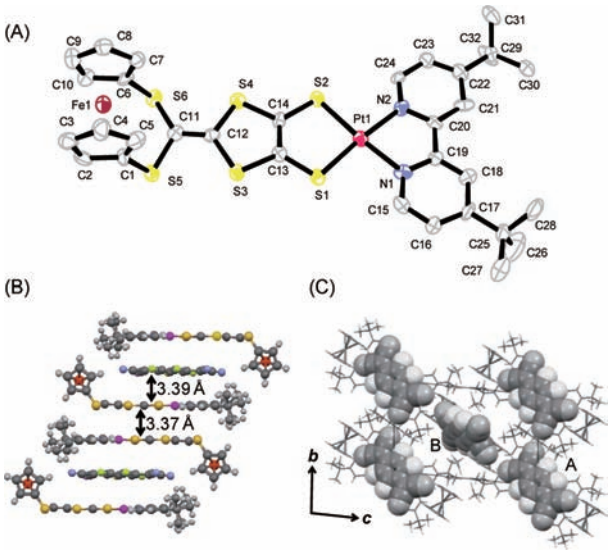

Figure 10. ORTEP drawing of $[FcS_4dt[Pt(^tBu_2bpy)]]^{\bullet+}$ with thermal ellipsoids set at 50% probability. Hydrogen atoms are omitted for clarity (a). 1D stacking structure formed by the cations and the anions (b), and positions of the anions A and B (shown in CPK model) in the crystal (c).

$(^tBu_2bpy)]$ removed an electron not from the ferrocene moiety but from the dithiolene moiety to produce the dithiolene-based π-radical. The dihedral angle between the C1S5S6C7 and S5S3S4S6 planes increased upon oxidation (Table 4). Similar planarization behavior was observed for the extended TTF derivatives BDT-TTP.[31] The neutral BDT-TTP formed a nonplanar molecular structure that transitioned to a planar structure upon oxidation, accompanying broader delocalization of the π-orbital. The same features are expected for $[FcS_4dt[Pt(^tBu_2bpy)]]^{\bullet+}$, in which enlargement of the dihedral angle caused delocalization of the dithiolene-based π-orbital across the bridging sulfur atoms S5 and S6, leading to stronger electronic communication between the ferrocene and dithiolene moieties. The change in the dihedral angle could explain why $[FcS_4dt[Pt(^tBu_2bpy)]]^{\bullet+}$ showed stronger electronic communication than $[FcS_4dt(Me)_2]^{\bullet+}$, although the molecular structure of the latter was not fully elucidated.

CONCLUSION

We developed a novel class of ferrocene–dithiolene hybrid molecules, $FcS_4dt(Me)_2$ and $FcS_4dt[Pt(^tBu_2bpy)]$. The physical properties and electronic structures of the complexes and their oxidized species $[FcS_4dt(Me)_2]^{\bullet+}$ and $[FcS_4dt[Pt(^tBu_2bpy)]]^{\bullet+}$ were investigated. The CV, EPR, and vis–NIR results indicated that a first oxidation process occurred at the ferrocene moiety for $FcS_4dt(Me)_2$, whereas oxidation occurred at the dithiolene moiety for $FcS_4dt[Pt(^tBu_2bpy)]$. This indicated that the distributions of the HOMO of $FcS_4dt(Me)_2$ and $FcS_4dt[Pt(^tBu_2bpy)]$ differed markedly, resulting in distinct spin density distributions of the oxidized species. These result indicated that the frontier orbital could be tuned by changing R in $FcS_4dt(R)_2$ (R = Me for $FcS_4dt(Me)_2$; 2R = $Pt(^tBu_2bpy)$ for $FcS_4dt[Pt(^tBu_2bpy)]$). Significant electronic communication between the ferrocene and dithiolene moieties was established for both the oxidized species $[FcS_4dt(Me)_2]^{\bullet+}$ and $[FcS_4dt[Pt(^tBu_2bpy)]]^{\bullet+}$, which was hardly observed for the previously reported ferrocene–dithiolene hybrid molecules. The electron coupling parameters H_{AB} and the adiabatic potential energy curves of $[FcS_4dt(Me)_2]^{\bullet+}$ and $[FcS_4dt[Pt(^tBu_2bpy)]]^{\bullet+}$ were estimated. We revealed that the electronic communication strength (H_{AB}), ICT direction, and electronic structure (MOs and potential energy curves) of FcS_4dt-based complexes could be controlled by changing the energy level of the dithiolene-based MOs. These results indicate that FcS_4dt-based metalladithiolenes can exhibit tunable electronic structures, which have never been achieved, that enable to develop new physical and chemical properties.

EXPERIMENTAL SECTION

General Method. Solvents and reagents were used as received from commercial sources unless otherwise noted. FcS_2CO and thione 1 in Scheme 1 were prepared according to the procedures reported in the literature.[8,9] Tetrahydrofuran was distilled over Na-benzophenone, and dichloromethane, hexane, and toluene were distilled over CaH_2 under an N_2 atmosphere, respectively. All syntheses were performed under N_2 or Ar atmospheres.

NMR, ESI-TOF MS, and UV–vis–NIR Spectroscopy. NMR spectra (^1H) were recorded on a Bruker DRX500 spectrometer. ESI-TOF mass spectra were recorded using a Micromass LCT spectrometer. Solution samples for UV–vis–NIR spectroscopy were prepared under an argon atmosphere. UV–vis–NIR spectra were recorded on a V-570 spectrometer (JASCO) using quartz cells with a path length of 1 cm.

Single Crystal X-ray Diffraction Analysis. The data for $FcS_4dt(Me)_2$ and $FcS_4dt[Pt(^tBu_2bpy)]$ were collected at 113 K on a Rigaku AFC10 diffractometer with a Rigaku Saturn CCD system equipped with a rotating-anode X-ray generator that emitted graphite-monochromated Mo Kα radiation (0.7107 Å). The data for $[FcS_4dt[Pt(^tBu_2bpy)]](F_4TCNQ)\cdot C_6H_{14}\cdot CH_2Cl_2$ were collected at 93 K on a Rigaku AFC10 diffractometer using a Rigaku Suturn 70 CCD system equipped with a RA-Micro7 HFM X-ray generator that

Table 4. Selected Bond Lengths of $FcS_4dt[Pt(^tBu_2bpy)]$ and $[FcS_4dt[Pt(^tBu_2bpy)]]^{\bullet+}$

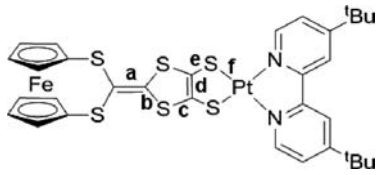

		a	*b*	*c*	*d*	*e*	*f*	dihedral angle[a]
exp	$FcS_4dt[Pt(^tBu_2bpy)]$	1.36(1)	1.755(9)	1.763(8)	1.34(1)	1.738(8)	2.266(2)	72
exp	$[FcS_4dt[Pt(^tBu_2bpy)]]^{\bullet+}$	1.34(2)	1.76(1)	1.75(1)	1.39(1)	1.70(1)	2.274(3)	57
calc (DFT)	$FcS_4dt[Pt(^tBu_2bpy)]$	1.363	1.778	1.777	1.348	1.756	2.328	65
calc (DFT)	$[FcS_4dt[Pt(^tBu_2bpy)]]^{\bullet+}$	1.369	1.771	1.749	1.392	1.726	2.344	52

[a]Dihedral angle between the C1S5S6C7 and S5S3S4S6 planes, shown in Figures 1c and 10a.

dx.doi.org/10.1021/ic300581a | *Inorg. Chem.* 2012, 51, 12102–12113

emitted Mo Kα radiation (0.7107 Å) and a Varimax Mo confocal mirror. A suitable single crystal was mounted on a looped film (micromount) using liquid paraffin. An empirical absorption correction using equivalent reflections and Lorentzian polarization correction was performed with the program Crystal Clear 1.3.6. The structure was solved using SIR-92,[22] and the whole structure was refined against F^2 using SHELXL-97.[23] All non-hydrogen atoms were refined anisotropically. Hydrogen atoms were located in idealized positions and were refined using a riding model with fixed thermal parameters. Pertinent crystallographic data were given in Supporting Information Table S1. In the case of $[FcS_4dt[Pt(^tBu_2bpy)]]$-$(F_4TCNQ)\cdot C_6H_{14}\cdot CH_2Cl_2$, abnormal anisotropic thermal displacement factors were detected for the carbon and nitrogen atoms C and N in the terminal CN bond on the F_4TCNQ anion. This abnormality presumably originated from the disorder of the dichloromethane molecule, because this CN bond was directed toward the disordered dichloromethane in the crystal and formed a hydrogen bond or a halogen bond between the N···H or N···Cl atoms.

DFT Calculations. The calculations were carried out using the Gaussian03 program package.[23] The geometries of the complexes were optimized using density functional theory (DFT) methods without symmetry constraints. For $FcS_4dt(Me)_2$, the BP86 level of theory[24] with Ahlrich's def2-SVP basis set[25] was used to model the Fe atom, and the 6-31G(d) basis set[26] was used to model the other atoms. The three-parametrized Becke–Lee–Yang–Parr (B3LYP) hybrid exchange–correlation functional[27] was used in the models of $FcS_4dt[Pt(^tBu_2bpy)]$ and $[FcS_4dt[Pt(^tBu_2bpy)]]^{\bullet+}$ using the LanL2DZ (Hay–Wadt ECP)[28] basis set for the Fe and Pt atoms and the 6-31G(d) basis set[26] for the other atoms. The stabilities of all optimized structures were confirmed by calculating the molecular vibrational frequencies, in which no imaginary frequencies were observed in any of the compounds. On the basis of the optimized structure of $[FcS_4dt[Pt(^tBu_2bpy)]]^{\bullet+}$, the TD-DFT method was applied to calculate the excited states relevant to the absorption spectra. The solvent effect (dichloromethane) was considered using the PCM model.

Cyclic Voltammetry. A glassy carbon (GC) rod (outside diameter 3 mm, Tokai Carbon GC-20) was embedded in Pyrex glass, and the cross section was used as a working electrode (polished with Al_2O_3 fine particles (0.3 μmϕ), washed with purified water and acetone with ultrasonication prior to use). Cyclic voltammetry was carried out under an argon atmosphere equipped with a platinum-wire counter electrode and an Ag^+/Ag reference electrode (10 mM $AgClO_4$ and 0.1 M $Bu_4N\cdot ClO_4$–MeCN solution) with an ALS-650B voltammetric analyzer. All potentials were reported vs the ferrocenium/ferrocene (ferrocenium/ferrocene) potential.

EPR Measurements. The EPR spectra were collected using a JEOL JES-RE2X. $FcS_4dt(Me)_2$ in dichloromethane (0.94 mM) was introduced into the sample tube, to which 1 mol equiv of tris(4-bromophenyl)ammoniumyl hexachloroantimonate in dichloromethane was added using a microsyringe at −78 °C. The obtained sample solution was degassed by three freeze–pump–thaw cycles. Finally, the tube was sealed under a vacuum.

Synthesis of $FcS_4dt(CH_2CH_2CN)_2$. FcS_2CO[8] (0.419 g, 1.52 mmol) and thione **1**[9] (0.603 g, 1.98 mmol) were suspended in toluene (3.5 mL) and $P(OEt)_3$ (13 mL) and were stirred for 2 h under reflux. After the reaction mixture was cooled down to r.t. to which hexane was added, the solution was kept overnight at −10 °C. The precipitate was filtered, washed with MeOH, and dried in vacuo. The resulting solid was purified by silica gel column chromatography (eluent: CH_2Cl_2). FcS_4dt (0.132 g) was obtained in 16% yield. Anal. calcd for $C_{20}H_{16}FeN_2S_6$: C, 45.10; H, 3.03; N, 5.26. Found: C, 44.83; H, 3.20; N, 5.06. ^1H NMR ($CDCl_3$ 500 MHz): δ 2.82 (t, 4H, J = 6.9 Hz), 3.11 (t, 4H, J = 6.9 Hz), 4.24 (m, 4H), 4.32 (m, 4H). MS (ESI-TOF+): m/z 532 $[FcS_4dt]^+$.

Synthesis of $FcS_4dt(Me)_2$. To a suspension of FcS_4dt (84.2 mg, 0.158 mmol) in dry MeOH (15 mL) and THF (6 mL) was added NaOMe (34.8 mg, 0.644 mmol), and the mixture was stirred for 2 h. MeI (75 μL, 0.16 mmol) was added, and the solution was further stirred for 1.5 h. The solvents were evaporated, and the resulting solids were dissolved in CH_2Cl_2, washed with water (3 times), and dried over Na_2SO_4. The resulting solution was filtered with SiO_2 and concentrated. A yellow solid was obtained by recrystallization from CH_2Cl_2–hexane in a 79% yield. Anal. Calcd for $C_{16}H_{14}FeS_6$: C, 42.28; H, 3.10; N, 0. Found: C, 42.10; H, 3.13; N, 0. ^1H NMR ($CDCl_3$ 500 MHz): δ 2.44 (s, 6H), 4.24 (m, 4H), 4.30 (m, 4H). MS (ESI-TOF+): m/z 454 $[FcS_4dt(Me)_2]^+$. A yellow crystal suitable for single crystal X-ray diffraction study was obtained by recrystallization from hot ethanol.

Synthesis of $FcS_4dt[Pt(^tBu_2bpy)]$. To a suspension of FcS_4dt (37.0 mg, 69.5 μmol) in dry MeOH (7 mL) and THF (5 mL) was added NaOMe (17.0 mg, 315 μmol). The mixture was stirred for 4 h, and $PtCl_2(^tBu_2bpy)$[11] (35.0 mg, 65.5 μmol) was added. The reaction mixture was evaporated after stirring overnight. The resulting blue solid was dissolved in CH_2Cl_2, washed with water (3 times), dried over $MgSO_4$, and concentrated in vacuo. The resulting precipitate was purified by silica gel column chromatography (eluent: CH_2Cl_2). $FcS_4dt[Pt(^tBu_2bpy)]$ (13.5 mg, 15.2 mmol) was obtained in a 22% yield. ^1H NMR ($CDCl_3$ 500 MHz): δ 1.46 (s, 18H), 4.25 (s, 8H), 7.46 (dd, 2H, J = 1.5 Hz, 6.1 Hz), 7.92 (d, 2H, J = 1.5 Hz), 8.90 (d, 2H, J = 6.1 Hz). HRMS (HR-ESI-TOF) m/z calcd for $C_{32}H_{32}FeN_2PtS_6$: 887.9888 $[FcS_4dt[Pt(^tBu_2bpy)]]^+$. Found: 887.9882. A deep blue crystal suitable for single crystal X-ray diffraction study was obtained by recrystallization from CH_2Cl_2–MeOH–hexane.

Synthesis of $[FcS_4dt[Pt(^tBu_2bpy)]](F_4TCNQ)\cdot C_6H_{14}\cdot CH_2Cl_2$. A solution of $FcS_4dt[Pt(^tBu_2bpy)]$ (7.9 mg, 8.9 μmol) and F_4TCNQ (2.6 mg, 8.9 μmol, 95% in purity) in CH_2Cl_2 (8 mL) was stirred for 2 h, followed by addition of hexane (24 mL). The resulting solid was collected by filtration and washed with hexane. A green solid (8.4 mg) was obtained by recrystallization from CH_2Cl_2–hexane at −10 °C in 81% yield. MS (ESI-TOF+): m/z observed 887.9896, calcd for $[FcS_4dt[Pt(^tBu_2bpy)]]^+$ 887.9895. (ESI-TOF-): m/z observed 276.0041, calcd for $[F_4TCNQ]^-$ 276.0059. A green crystal suitable for single crystal X-ray diffraction study was obtained by evaporating the solvent from the CH_2Cl_2–hexane solution at −10 °C.

■ ASSOCIATED CONTENT

Ⓢ Supporting Information

X-ray crystallographic information files (CIF) for $FcS_4dt(Me)_2$, $FcS_4dt[Pt(^tBu_2bpy)]$, and $[FcS_4dt[Pt(^tBu_2bpy)]]$-$(F_4TCNQ)\cdot C_6H_{14}\cdot CH_2Cl_2$; voltammograms of $FcS_4dt[Pt(^tBu_2bpy)]$, EPR spectra of $[FcS_4dt(Me)_2]^{\bullet+}$, deconvolution of vis–NIR spectrum for $[FcS_4dt[Pt(^tBu_2bpy)]]^{\bullet+}$, crystal data, and the tables of optical parameters calculated by the TD-DFT method. This material is available free of charge via the Internet at http://pubs.acs.org.

■ AUTHOR INFORMATION

Corresponding Author

*E-mail: nisihara@chem.s.u-tokyo.ac.jp.

Notes

The authors declare no competing financial interest.

■ ACKNOWLEDGMENTS

We thank the Research Hub Advanced Nano Characterization (Graduate School of Engineering, The University of Tokyo) for the single crystal X-ray diffraction studies of $[FcS_4dt[Pt(^tBu_2bpy)]](F_4TCNQ)\cdot C_6H_{14}\cdot CH_2Cl_2$. This work was supported by Grants-in-Aid from MEXT Japan (Nos. 20245013 and 21108002, area 2107 (Coordination Programming)) and the Global COE Program for Chemistry Innovation.

■ REFERENCES

(1) (a) Stiefel, E. I.; Karlin, K. D. *Progress in Inorganic Chemistry, Dithiolene Chemistry: Synthesis, Properties, and Applications*; Wiley-

Interscience, 2003, 52. (b) Cassoux, P. *Coord. Chem. Rev.* **1999**, *185*−*186*, 213−232. (c) Yamashita, S.; Yamamoto, T.; Nakazawa, Y.; Tamura, M.; Kato, R. *Nature Commun.* **2011**, *2*, 275/1−275/6. (d) Kato, R. *Chem. Rev.* **2004**, *104*, 5319−5346. (e) Kobayashi, A.; Fujiwara, E.; Kobayashi, H. *Chem. Rev.* **2004**, *104*, 5243−5264. (f) Kobayashi, A.; Okano, Y.; Kobayashi, H. *J. Phys. Soc. Jpn.* **2006**, *75*, 051002−1−051002−12. (g) Kosaka, Y.; Yamamoto, H. M.; Nakao, A.; Tamura, M.; Kato, R. *J. Am. Chem. Soc.* **2007**, *129*, 3054−3055. (h) Zuleta, J. A.; Bevilacqua, J. M.; Proserpio, D. M.; Harvey, P. D.; Eisenberg, R. *Inorg. Chem.* **1992**, *31*, 2396−2404. (i) Cummings, S. D.; Eisenberg, R. *J. Am. Chem. Soc.* **1996**, *118*, 1949−1960. (j) Cummings, S. D.; Cheng, L. T.; Eisenberg, R. *Chem. Mater.* **1997**, *9*, 440−450. (k) Muellerwesterhoff, U. T.; Vance, B.; Yoon, D. I. *Tetrahedron* **1991**, *47*, 909−932. (l) Fabian, J.; Nakazumi, H.; Matsuoka, M. *Chem. Rev.* **1992**, *92*, 1197−1226. (m) Curreli, S.; Deplano, P.; Faulmann, C.; Ienco, A.; Mealli, C.; Mercuri, M. L.; Pilia, L.; Pintus, G.; Serpe, A.; Trogu, E. F. *Inorg. Chem.* **2004**, *43*, 5069−5079. (n) Kusamoto, T.; Kume, S.; Nishihara, H. *J. Am. Chem. Soc.* **2008**, *130*, 13844−13845. (o) K. P. Rao, K. P; Kusamoto, T.; Sakamoto, R.; Yamamoto, Y.; Kume, S.; Nihei, M.; Oshio, H.; Nishihara, H. *Chem. Commun.* **2011**, *47*, 2330−2332.

(2) (a) Wang, K.; Stiefel, E. I. *Science* **2001**, 106−109. (b) Harrison, D. J.; Nguyen, N.; Lough, A. J.; Fekl, U. *J. Am. Chem. Soc.* **2006**, *128*, 11026−11027. (c) Zhang, J.; Du, P. W.; Schneider, J.; Jarosz, P.; Eisenberg, R. *J. Am. Chem. Soc.* **2007**, *129*, 7726−7727. (d) Kusamoto, T.; Kume, S.; Nishihara, H. *Angew. Chem., Int. Ed.* **2010**, *49*, 529−531. (e) McNamara, W. R.; Han, Z.; Alperin, P. J.; Brennessel, W. W.; Holland, P. L.; Eisenberg, R. *J. Am. Chem. Soc.* **2011**, *133*, 15368−15371.

(3) Ray, K.; Petrenko, T.; Wieghardt, K.; Neese, F. *Dalton Trans.* **2007**, 1552−1566 and references therein..

(4) (a) D'Alessandro, D. M.; Keene, F. R. *Chem. Soc. Rev.* **2006**, *35*, 424−440. (b) Ratera, I.; Sporer, C.; Ruiz-Molina, D.; Ventosa, N.; Baggerman, J.; Brouwer, A. M.; Rovira, C.; Veciana, J. *J. Am. Chem. Soc.* **2007**, *129*, 6117−6129. (c) Huesmann, H.; Förster, C.; Siebler, D.; Gasi, T.; Heinze, K. *Organomet.* **2012**, *31*, 413−427. (d) Gispert, J. R. *Coordination Chemistry*; Wiley-Interscience: New York, 2008, *403*.

(5) (a) Hush, N. S. *Prog. Inorg. Chem.* **1967**, *8*, 391−444. (b) Hush, N. S. *Electrochim. Acta* **1968**, *13*, 1005−1023.

(6) (a) Kondo, M.; Uchikawa, M.; Namiki, K.; Zhang, W. W.; Kume, S.; Nishibori, E.; Suwa, H.; Aoyagi, S.; Sakata, M.; Murata, M.; Kobayashi, Y.; Nishihara, H. *J. Am. Chem. Soc.* **2009**, *131*, 12112−12124. (b) Kondo, M.; Uchikawa, M.; Zhang, W. W.; Namiki, K.; Kume, S.; Murata, M.; Kobayashi, Y.; Nishihara, H. *Angew. Chem., Int. Ed.* **2007**, *46*, 6271−6274. (c) Rao, K. P.; Kondo, M.; Sakamoto, R.; Kusamoto, T.; Kume, S.; Nishihara, H. *Chem. Lett.* **2011**, *40*, 1456−1458. (d) Sakamoto, R.; Rao, K. P.; Nishihara, H. *Chem. Lett.* **2011**, *40*, 1316−1326. (e) Rao, K. P.; Kondo, M.; Sakamoto, R.; Kusamoto, T.; Nishikawa, M.; Kume, S.; Nihei, M.; Oshio, H.; Nishihara, H. *Chem.—Eur. J.* **2011**, *17*, 114010−14019.

(7) (a) Wilkes, S. B.; Butler, I. R.; Underhill, A. E.; Hursthouse, M. B.; Hibbs, D. E.; Malik, K. M. A. *J. Chem. Soc., Dalton Trans.* **1995**, 897−903. (b) Wilkes, S. B.; Butler, I. R.; Underhill, A. E.; Kobayashi, A.; Kobayashi, H. *J. Chem. Soc., Chem. Commun.* **1994**, 53−54. (c) Lee, H.-J.; Noh, D.-Y. *J. Mater. Chem.* **2000**, *10*, 2167−2172. (d) Mueller-Westerhoff, U. T.; Sanders, R. W. *Organometallics* **2003**, *22*, 4778−4782.

(8) Herberhold, M.; Brendel, H. D. *J. Organomet. Chem.* **1993**, *458*, 205−209.

(9) Misaki, Y.; Nishikawa, H.; Kawakami, K.; Koyanagi, S.; Yamabe, T.; Shiro, M. *Chem. Lett.* **1992**, *21*, 2321−2324.

(10) Fabre, J. M. *Chem. Rev.* **2004**, *104*, 5133−5150.

(11) Egan, T. J.; Koch, K. R.; Swan, P. L.; Clarkson, C.; Schalkwyk, D. A. V.; Smith, P. J. *J. Med. Chem.* **2004**, *47*, 2926−2934.

(12) Saito, G.; Yoshida, Y. *Chem. Rec.* **2011**, *11*, 124−145.

(13) Kusamoto, T. Ph.D. Dissertation, The University of Tokyo, 2010.

(14) El-Wareth, A.; Sarhan, A. O. *Tetrahedron* **2005**, *61*, 3889−3932 and references therein.

(15) Ushijima, H.; Akiyama, T.; Kajitani, M.; Shimizu, K.; Aoyama, M.; Masuda, S.; Harada, Y.; Sugimori, A. *Bull. Chem. Soc. Jpn.* **1990**, *63*, 1015−1019.

(16) Prins, R. *Mol. Phys.* **1970**, *19*, 603−620.

(17) (a) Connick, W. B.; Gray, H. B. *J. Am. Chem. Soc.* **1997**, *119*, 11620−11627. (b) Cocker, T. M.; Bachman, R. E. *Inorg. Chem.* **2001**, *40*, 1550−1556. (c) Pap, J. S.; Benedito, F. v. L; Bothe, E.; Bill, E.; George, S. D.; Weyhermüller, T.; Wieghardt, K. *Inorg. Chem.* **2007**, No. 46, 4187−4196.

(18) Among many ferrocene−(metalla)dithiolenes in refs 7 and 14, a ferrocene−TTF hybrid reported by Iyoda et al. [*Chem. Lett.* **2001**, *40*, 1550−1556] was one rare example to display a broad NIR absorption indicative of ICT between the two redox centers. It should be noted that the unique ferrocene−dithiolene hybrid, in which the ferrocene unit was borrowing its second π-system from the dithiolene backbone, exhibited NIR absorption ascribed to ICT. Harrison, D. J.; De Crisci, A. G.; Lough, A. J.; Kerr, M. J.; Fekl, U. *Inorg. Chem.* **2008**, *47*, 10199−10201.

(19) Meneghetti, M.; Pecile, C. *J. Chem. Phys.* **1986**, *84*, 4149−4162.

(20) Dong, T.-Y.; Lin, H.-M.; Hwang, M.-Y.; Lee, T.-Y.; Tseng, L.-H. *J. Organomet. Chem.* **1991**, *414*, 227−244.

(21) Lim, B. S.; Fomitchev, D. V.; Holm, R. H. *Inorg. Chem.* **2001**, *40*, 4257−4262.

(22) Altomare, A.; Burla, M. C.; Camalli, M.; Cascarano, G. L.; Giacovazzo, C.; Guagliardi, A.; Moliterni, A. G. G.; Polidori, G.; Spagna, R. *J. Appl. Crystallogr.* **1999**, *32*, 115−119.

(23) (a) Sheldrick, G. M. *SHELX-97*, A Program for Crystal Structure Analysis, release 97-2; University of Göttingen, Germany, 1997. (b) Frisch, M. J., et al. *Gaussian 03*, revision-B.05; Gaussian, Inc.: Pittsburgh, PA, 2003.

(24) (a) Becke, A. D. *Phys. Rev. A* **1988**, *38*, 3098−3100. (b) Perdew, J. P. *Phys. Rev. B.* **1986**, *33*, 8822−8824.

(25) Weigend, F.; Ahlrichs, R. *Phys. Chem. Chem. Phys.* **2005**, *7*, 3297−3305.

(26) Hariharan, P. C.; Pople, J. A. *Theor. Chim. Acta* **1973**, *28*, 213−222.

(27) Becke, A. D. *J. Chem. Phys.* **1993**, *98*, 5648−5652.

(28) Hay, P. L.; Wadt, W. R. *J. Chem. Phys.* **1985**, *82*, 270−283.

(29) Kubo, K.; Nakano, M.; Tamura, H.; Matsubayashi, G. E. *Inorg. Chim. Acta* **2002**, *336*, 120−124.

(30) Metzger, R. M.; Heimer, N. E.; Gundel, D.; Sixl, H.; Harms, R. H.; Keller, H. J.; Nothe, D.; Wehe, D. *J. Chem. Phys.* **1982**, *77*, 6203−6214.

(31) Misaki, Y. *Sci. Technol. Adv. Mater.* **2009**, *10*, 024301−22.

(32) Quasi-reversibility is thought to originate from the insoluble compounds formed on the surfaces of working electrodes during an oxidation process. After the CV measurement, the working electrode was washed with dichloromethane several times and the CV was measured again using a blank solution (0.1 M $Bu_4N{\cdot}ClO_4$ in CH_2Cl_2). Small irreversible redox waves with potentials similar to those of the sample were observed, indicating the presence of insoluble compounds on the electrode surface.

(33) Sato, O.; Tao, J.; Zhang, Y. Z. *Angew. Chem., Int. Ed.* **2007**, *46*, 2152−2187.

(34) To estimate a degree of electrostatic effects from the positive charge on the ferrocene unit, we focused on the electrochemical properties of a ferrocene−dithiolene conjugate **Fc-TTF** discussed in ref 18 [*Chem. Lett.* **2001**, 1310−1311], in which ferrocene was directly bound to the TTF skeleton via a single sigma-bond. The reduction potential of the 3rd oxidation process ($E^3_{1/2\text{Fc-TTF}}$) for **Fc-TTF**, which corresponds to the second oxidation of the TTF moiety with a positive charge on the ferrocenium unit, was compared with a reduction potential ($E^2_{1/2\text{TTF}}$) at which the second oxidation of TTF molecule occurred. The difference was 0.11 V between $E^3_{1/2\text{Fc-TTF}}$ and $E^2_{1/2\text{TTF}}$. This difference originates mainly from the electrostatic effects from the positive charge on the ferrocenium moiety. Such electrostatic effects weaken as the distance (r) between the ferrocene and the dithiolene units elongate, according to the fact that Coulomb interaction is proportional to $1/r$. In the parent compound $FcS_4dt(Me)_2$, the

distance between the two units are longer than **Fc-TTF**, thus the electrostatic effects from the positive charge on the ferrocenium unit should be smaller (<0.11 V). On the other hand, the difference between $E_2^{0'ox}$ of $FcS_4dt(Me)_2$ and $E_1^{0'ox}$ of $chxdt(CH_2CH_2CN)_2$ was 0.24 V, which was larger than 0.11 V. This result indicated that both the electrostatic interaction and the electronic communication affected the electrochemical properties in $FcS_4dt(Me)_2$.

(35) The Pt complex was represented as $FcS_4dt[Pt(^tBu_2bpy)]$ according to the formula $FcS_4dt(R)_2$, although Pt(diimine)(dithiolate) is a common description for this kind of compound.

(36) Makedonas, C.; Mitsopoulou, A. C.; Lahoz, J. F.; Balana, I. A. *Inorg. Chem.* **2003**, *42*, 8853−8865.